Copy 657

[redacted] NASA TM X-316

NASA TM X-316

CASE FILE COPY

CLASSIFICATION CHANGED
UNCLASSIFIED
By Authority of TD 71-635 Date 18 OCT 1971

TECHNICAL MEMORANDUM

X-316

Declassified by authority of NASA
Classification Change Notices No. 215
Dated **31 DEC 1971

FLOW FIELDS, PRESSURE DISTRIBUTIONS, AND HEAT TRANSFER FOR DELTA WINGS AT HYPERSONIC SPEEDS

By Mitchel H. Bertram, William V. Feller,
and James C. Dunavant

Langley Research Center
Langley Field, Va.

[redacted]

[redacted]

[redacted]

NATIONAL AERONAUTICS AND SPACE ADMINISTRATION
WASHINGTON September 1960

[redacted]

1M

[redacted]

NATIONAL AERONAUTICS AND SPACE ADMINISTRATION

TECHNICAL MEMORANDUM X-316

FLOW FIELDS, PRESSURE DISTRIBUTIONS, AND HEAT TRANSFER FOR DELTA WINGS AT HYPERSONIC SPEEDS*

By Mitchel H. Bertram, William V. Feller,
and James C. Dunavant

L
1
0
4
2

SUMMARY

Successful correlations of pressure on delta-planform wings are shown for both the center-line and spanwise pressure distributions over a range of sweep, Mach number, angle of attack, and dihedral angle. Such correlations allow the application of experimental results to Mach numbers widely different from those at which the data were obtained, thus allowing the prediction of the pressure on the lifting surface of a vehicle such as the Dyna-Soar with confidence. Much of the heat transfer has been found to be amenable to simple approaches which take into account the flow pattern peculiar to the angle-of-attack range under consideration. The leading edge itself has been found to become a trailing edge in the sense of airflow direction at high angles of attack. This is connected with the appearance of conical flow on the delta wing and tends to alleviate the heat transfer to the leading edge.

INTRODUCTION

The delta planform is a type of great interest in hypersonic-glider and lifting-reentry studies. In order to supply the information necessary for the proper evaluation and successful application of this shape an extensive research program has been carried out.

Only a small fraction of the results so far obtained can be treated here; however, it will be the purpose of this paper to give the highlights of the recent research results.

SYMBOLS

a_o	speed of sound, reservoir
c	chord

---

*Title, Unclassified. [redacted]

[redacted]

h	heat-transfer coefficient
h_{MAX}	heat-transfer coefficient on stagnation point
l	length along leading edge
M	Mach number
N_{St}	Stanton number based on free-stream conditions
p	pressure
p_{MAX}	stagnation pressure behind a normal shock
R	Reynolds number
s	distance along surface from geometric stagnation point of spherical nose
t	thickness
u	velocity
x	chordwise distance
α	angle of attack of plane of leading edges
α_{EFF}	local angle of attack of the wing panel (eq. (1))
β	angle of shock from stream
ζ	surface flow angle measured from center line
θ	ray angle from center line
Γ	dihedral angle
Λ	sweep angle

Subscripts:

c	chord
℄	center line
le	leading edge

[redacted]

x	chordwise distance from leading edge
∞	free stream

FLOW FIELDS AND PRESSURE DISTRIBUTIONS

Examples of the models tested are shown in figures 1 and 2. Most of the investigations were concerned with flat or slab delta wings; however, as illustrated in figure 1 a set of models was designed to investigate the effect of dihedral on the underside of the wing.

Models shown in figure 2 are examples of wings with a large amount of blunting which are part of a coordinated delta-wing program. All the models in this program were of this type - that is, a slab with a swept-cylinder leading edge - and many were tested with the two different noses shown here. The length of the wing in terms of diameters varied from facility to facility. For instance, although the models shown in figure 2, which were tested in the Langley 11-inch hypersonic tunnel, are 7 diameters long, the model tested in the Unitary Plan wind tunnel at the Langley Research Center was 20 diameters long.

In figure 3 are presented schlieren photographs of the shock shape on the cylindrical-leading-edge blunt-nose model in top view in order to show the extent of the effect of the blunt nose. In figure 3(a) the model is at zero angle of attack at Mach 6.9 and 9.6 in air and Mach 18.4 in helium. In figure 3(b) the angle of attack ranges from 10° to 30° at Mach 6.9 in air. The bottom wing is 21 diameters long and the top wing corresponds to a 3 times enlargement of that part of the bottom wing ahead of the dashed line. This top wing is only 7 diameters long. At zero angle of attack the Mach 6.9 and 9.6 pictures are very similar, and the shock shape is much the same at Mach 18.4 in helium. If the extent of the nose influence is judged by the inflection in the leading-edge shock, the blunt nose affects less of the wing length as the angle of attack increases. Since the spherical nose has a shock of fixed shape, that is, independent of angle of attack in the range shown here, this change in shock shape is mainly due to changes in the shock around the cylindrical leading edge with angle of attack. Far enough away from the nose, at 0° and 10° angle of attack, the shock is parallel to the leading edge. At 20° and, to a more noticeable extent, at 30° angle of attack the main-stream flow senses the local wing span, and the leading-edge shock shape becomes conical in nature.

[redacted]

Next, the shock is examined in side view. In this case figure 4 presents the shock angle determined from schlieren photographs of the flat wings as a function of angle of attack. Included in this figure but not identified are wings with sharp and blunt noses and leading edges. To avoid data with substantial pressure gradients, data at angles of attack less than about 20° for the blunted wings and within about $1\frac{1}{2}$ diameters of the nose are excluded from this figure. These exclusions are not very limiting because the main interest is in applications of the delta wing in the range of angle of attack from 15° to 50° on reentry vehicles. The location of the wing surface and two-dimensional oblique-shock theory are included in this figure for reference. Note that while for shock angles greater than about 19° the delta-wing shock angles deviate considerably from the two-dimensional theory, the incremental effect of Mach number seems to be given with good accuracy by the theory, and it is expected that with further increases in Mach number there will be an almost negligible change in shock angle. Also noteworthy is the insensitivity of the shock angle to changes in sweep angle and the small shock standoff angle from the wing surface.

As yet there are no adequate theories for predicting the pressures on delta wings with detached shocks. However, this fact does not preclude a correlation of empirical results. Figure 5 shows the wall-to-free-stream static-pressure ratios obtained on the center line of various flat wings. Only data where essentially no longitudinal pressure gradient exists on the center line have been included. The Mach 6.85 and 9.6 data encompass the range of angle of attack up to about 60°. For the flat wings the sweep angles at which pressure data are available are only 70° and 75°; however, data for delta wings with sweep angles to at least as low as 60° should correlate with the results shown here. The pressure ratio does not appear to vary with leading-edge bluntness, nose shape, or sweep angle. Figure 6 shows the good correlation which results from using the hypersonic similarity parameter $M_\infty \sin \alpha$ suggested by both hypersonic oblique shock theory and Newtonian theory to correlate the wall-to-free-stream static-pressure ratio for the same data. Included in these figures are the results from exact two-dimensional oblique shock theory and Newtonian theory for reference.

The pressure data from wings with dihedral on the underside are shown in figure 7 and these data correlate well with flat-wing data. Data obtained for a 60° swept wing are included here. For these data the angle of attack used in the correlating parameter is the local angle of attack of the wing panel given by the following equation:

$$\tan \alpha_{EFF} = \tan\left[\alpha + \text{arc tan}\left(\tan \theta_{le} \tan \Gamma\right)\right] \frac{\dfrac{\cos \alpha}{\tan \Gamma}}{\sqrt{1 + \dfrac{\cos^2 \alpha}{\tan^2 \Gamma}}} \qquad (1)$$

[redacted]

L-1042

[redacted]

With this correlation the center-line pressures on a delta wing may be predicted at Mach numbers considerably different from those of the tests.

Up to now consideration has been given to wings at angles of attack high enough so that no longitudinal pressure gradient exists on the center line of the wing. The question arises as to what extent the center-line pressures are altered in the region of the nose. Figure 8 examines in some detail the center-line pressure distribution on the hemisphere-nose delta wing of 70° sweep. This wing had swept cylinders forming the leading edges, and overall the wing corresponded to the first few feet of an actual hypersonic glider. The data are shown over a range of angle of attack from 0° to 20°. In this figure the pressure parameter is p/p_{MAX} where p_{MAX} is the stagnation pressure after a normal shock. The distance parameter is distance along the surface on the center of the wing in terms of leading-edge diameters. The origin of the surface distance is always taken at the geometric stagnation point of the spherical nose. On the spherical nose there is a Mach number freeze; that is, p/p_{MAX} is a function only of position on the sphere, not of free-stream Mach number. On the slab portion of the high-pressure side of the wing the pressure gradient induced by the blunt nose, which is so pronounced at zero angle of attack, becomes less severe with increasing angle of attack and virtually disappears at 20° angle of attack and greater. (See ref. 1.)

Thus far only the center line of the wing has been considered. The flow over the wing will now be examined in a more general way. Figure 9 shows tracings of surface flow streamlines formed by flowing lubricating oil impregnated with carbon black on a sharp-leading-edge wing with 75° sweep at Mach 9.6. At $\alpha = 0^\circ$ there is a surface flow in toward the center of the wing caused by the pressure gradient induced by the thick boundary layer. However, because of this very gradient, the streamlines external to the boundary layer must be out away from the center of the wing. With increasing angle of attack, as shock-loss effects start to predominate, the flow at the surface also turns out from the center. At 15° angle of attack the flow is away from the wing center line but it still comes in across the leading edge. At 30° angle of attack the flow has turned out to such an extent that in the sense of airflow direction the geometric leading edge has become a trailing edge. An interesting feature of the flow at 30° angle of attack is the appearance of a parting line at about 12° out from the center line of the wing. At 60° angle of attack the flow lines, which for the most part were more or less straight at 15° and 30° angle of attack, appear to be hyperbolic in nature. The parting line referred to at 30° angle of attack has moved into the center of the wing. More detail on these flows is shown in figure 10. Here the surface flow angles measured from these oil flow streaks are shown as a function of ray angle from the apex. This figure shows the movement of the parting line into the center of the wing. A line for perfect radial

[redacted]

flow has been put on the figure for reference. The location of the parting line is given by the point at which the data cross the line for radial flow. Note that the flow lines are very nearly radial in the central region of the wing at 45° angle of attack, and thus at higher angles of attack than this there is no parting line as such, unless one wishes to view the center line of the delta wing as a parting line.

At this point the effect of dihedral on the surface flow angularity will be examined. Shown in figure 11 are results from the 75° swept sharp-leading-edge wing at 30° angle of attack with dihedral angles of 0° and 26°. The angles of the oil-carbon black streaks relative to the center line of the wing are shown as a function of angular measure from the wing center line. The curves, which are fairings of the measurements, have been made exactly parallel to each other. That this can be done indicates that the spanwise pressure distributions should not be a function of dihedral angle. In addition, such an approach as the use of the local angle of attack of the surface in correlating wing pressures is also partially justified.

Figure 12 shows the lateral pressure distributions associated with these flow patterns from 0° to 60° angle of attack. The local pressure in every case has been divided by the pressure on the center line of the wing. Included in this figure are data for two Mach numbers, two sweep angles, and two dihedral angles. Overall one may note the insensitivity of the lateral pressure distributions at angle of attack to variations in any of these parameters. At 30° and 60° angle of attack the flow is conical, as indicated by oil flow tracings, and at the highest angle of attack (60°) the pressure distribution approaches that for a disk at 90° angle of attack to a hypersonic flow, to which it is compared in this figure. At zero angle of attack the pressures are high in the leading-edge region because of boundary-layer displacement effects and the flow is not conical.

Insofar as pressures are concerned successful correlations have been shown for both the center-line and spanwise pressure distributions in which the effect of a modification such as the addition of dihedral to the surface is included. Such correlations allow the application of experimental results to Mach numbers widely different from those at which the data were obtained, thus allowing the prediction of the pressure on the lifting surface of a vehicle such as the Dyna-Soar with confidence.

[redacted]

HEAT TRANSFER

This section will present some of the heat-transfer results from the broad study of delta wings described in the preceding section. Heat-transfer data on some of the configurations were available from $M = 3.5$ to about $M = 18$ from a number of facilities. The lower Mach number tests, however, showed transitional and turbulent flow over much of the surface, and at the highest Mach number the range of angles of attack and configurations studied was less complete. In order to present a clear picture of the overall distribution of heat-transfer rates and their relation to the external flow fields, the present discussion will be based mostly on the fully laminar data at $M = 9.6$ from the Langley 11-inch hypersonic tunnel.

The sharp-leading-edge delta wing will be considered first. It is geometrically simpler, but still indicates the general behavior of the heat transfer to the blunt wing for regions far from the nose and leading edges. Figure 13 shows the trend of heat transfer with angle of attack. The data are for points along the center line of a flat delta wing, presented in the form of the laminar flat-plate correlating parameter $N_{St}\sqrt{R_x}$ based on distance from the nose, with fluid properties evaluated at free-stream conditions.

Up to about 20° the heat transfer increases with angle of attack about as expected for a flat plate, as shown by the solid curve labeled "strip theory." At higher angles of attack, the data depart from the strip-theory trend and approach the dashed curve predicted by cross-flow theory, which regards the wing as a succession of independent spanwise strips in cross flow. For this theory, the component of free-stream velocity normal to the wing was used as the cross-flow stream, and the equivalent stagnation-point velocity gradient was calculated from a correlation of experimental pressure distributions measured on circular disks normal to the flow, which will be discussed later in this paper. This assumed pressure distribution does not fit the pressures measured on the delta wing at angles of attack of 30° and less, as was shown in figure 12 but becomes a better approximation at higher angles, and fits very well at $\alpha = 60^\circ$. The cross-flow approach also neglects completely effects of the chordwise component of the flow. A more refined and more nearly correct approach is given by the streamline divergence theory shown by the dot-dashed line. This method, based on the theory of Vaglio-Laurin (ref. 2) involves integrating along streamlines a quantity including local flow conditions and a term expressing the rate of separation or divergence of the streamlines. When the same spanwise component velocities are used as were used in the cross-flow theory to compute the streamlines near the wing center line, the Vaglio-Laurin

[redacted]

theory gives a very good prediction of the heat-transfer rates from about 25° to 60° angle of attack.

The theory of Vaglio-Laurin is actually very general and can be applied whenever the streamlines and flow properties outside the boundary layer are known. Because there is as yet no adequate theoretical method for determining the streamlines over the entire delta wing at all angles of attack, the application of this method will not be discussed further in this paper.

Above about 60°, where the wing shock is curved, the correlation based on the single characteristic length, the distance from the nose, can be expected to break down. The behavior at angles near 90° is discussed further in reference 3. The viscous interaction effects on the wing will be most important near zero angle of attack. Previous studies indicate that the pressure induced by the boundary-layer growth would lead to higher heat-transfer rates than those on a flat plate with constant pressure, but the data near $\alpha = 0^{\circ}$ are in fact mostly lower. This behavior is examined more closely in figure 14. These data are for points all over the delta wing, plotted against streamwise distance from the leading edges in terms of root chord, and are shown for three Mach numbers. Near the leading edge, the heat transfer is increased by the induced pressure and pressure gradient as expected at the higher Mach numbers, but falls off to values below those predicted for a flat plate without induced pressure, and the decrease is greatest at the highest Mach numbers where the induced pressures are highest.

L
1
0
4
2

The explanation is found in the flow patterns shown in figure 15. The calculated streamlines outside the boundary layer, shown by the solid lines, are deflected outward and are slightly divergent, which would indicate an increased heat transfer. In the boundary layer near the surface, however, the induced pressure gradients produce a flow toward the center from each leading edge, shown by the dashed lines which are traced from oil streak patterns. This secondary flow piles up low-energy air in the middle of the wing, which thickens the boundary layer there and reduces the heat-transfer rates.

Because the pressure gradients producing this secondary flow decrease with distance from the leading edge, the effect should disappear some distance downstream of the nose of the wing. Available data do not, however, permit an assessment of how far downstream the reduction extends. The effect decreases with angle of attack and is negligible above about 12° at $M = 9.6$.

The spanwise distribution of heat-transfer coefficients on the sharp-leading-edge delta wing is shown in figure 16. Here, the experimental Stanton numbers along each of several spanwise lines are correlated by

[redacted]

taking the ratio of the measured values to the value calculated for the center-line point as though it were part of a flat plate at the same angle of attack as the wing. The curves labeled "strip theory" are included to give a frame of reference. They show the expected effect of the decreasing distance from the leading edge as the point considered moves out spanwise, assuming the streamlines to be straight and parallel, as on a strip of a flat plate.

At zero angle of attack, the heat transfer is high near the leading edge because of the boundary-layer induced pressure. The reduction discussed in figure 15 due to the inward flow near the surface extends over about half the semispan.

At 16° angle of attack, on the lower surface the flow is slightly outward, but the divergence of the streamlines is small and the heat transfer is fairly well predicted by simple strip theory.

At higher angles of attack, shown in figure 17, the pattern changes. The surface flows at $\alpha = 26^{\circ}$ and 45° on the lower surface show a region with nearly radial streamlines over most of the wing but with an outer region where the flow is outward over the leading edge. For this kind of flow, the uniform parallel flow assumed in the strip theory is clearly inadequate, and in fact the measured heat-transfer distributions resemble more nearly the shapes predicted by the cross-flow theory. The cross-flow pattern is not fully achieved, however, at 45° angle of attack. By $\alpha = 60^{\circ}$, as shown in figure 9 the central region of nearly radial flow has disappeared, and here the cross-flow theory gives a good prediction of the heat-transfer rates.

In figure 7 it was shown that the pressures on a dihedraled wing can be correlated with those for a flat plate by using the local wing panel angle of attack. In figure 18 the heat-transfer rates on three dihedraled wings are compared at the same wing panel angle of attack, 26°, and therefore at the same pressure. The flat wing (zero dihedral) data taken from figure 17 are shown by the shaded band. The heat transfer near the center line is considerably increased by the presence of dihedral, by as much as a factor of 2 at 26° dihedral. This is due to the outward component of the flow produced by the dihedral (shown in fig. 11) which thins the boundary layer near the center. The increment in heat transfer due to the dihedral falls off spanwise, and the outer half of the wing panel shows only small differences in heat transfer with dihedral. Thus, for the same lift and planform area a dihedraled wing will have a greater heat load than a flat one.

The discussion thus far has dealt with the behavior of sharp-leading-edge delta wings. The nose and leading edges of flight vehicles will necessarily be blunted to some extent. Far from the nose and leading

[redacted]

edges, the trends shown by the sharp wing are generally applicable to the blunt wing also. The heat transfer close to the nose is shown in figure 19. Here, heat-transfer coefficients measured at points along the center line of a spherical-nosed delta wing, expressed as a fraction of the value calculated for the stagnation point of a sphere, are plotted against surface distance from the stagnation point. On the sphere the measured heat-transfer rates agree well with the values calculated by Lees' theory (ref. 4) over the range of angles of attack presented. On the slab, at zero angle of attack figure 8 showed that the pressures induced by the spherical nose extend back over the entire length of this rather short model. The heat-transfer coefficients in figure 19 are also increased but are fairly well predicted by two-dimensional hypersonic similarity theory (ref. 5), which takes into account the pressure and pressure-gradient effects. As the angle of attack increases, the distance over which the induced pressures due to the nose are significant decreases, as was shown in figure 8, and by 21° the heat transfer on the lower surface of the slab is satisfactorily predicted by the constant-pressure strip theory from about 2 or 3 diameters back from the stagnation point.

At higher angles of attack, the flow becomes outward over the leading edge, and the cross-flow type of calculations should be appropriate. At 42° angle of attack, the cross-flow theory in fact gives a good prediction of the center-line heat-transfer rates. The spanwise velocity gradients used for the cross-flow theory calculations were obtained from the velocity distributions shown in figure 20. These were computed from pressure measurements on flat-faced disks normal to the flow, with various corner radii, ranging from the sharp edge to the hemisphere. It was found that the velocity gradients near the center line seemed to vary linearly with the ratio of corner radius to overall diameter, and could be very well represented by the equation:

$$\frac{D}{a_o}\frac{du}{dx}\bigg|_{x=0} = 0.745 + 3.14\frac{r}{D}$$

This relation was assumed to be applicable to the delta wing near the center line, with the local span and cylinder radius as D and r, respectively, and using the speed of sound at the fictitious stagnation temperature corresponding to the total energy of the normal component flow.

The cylindrical leading edge of a wing at low angles of attack is usually treated as part of an infinite cylinder. The changes in flow direction of the surface streamlines with angle of attack and the proximity of the blunt nose suggest a limitation to the validity of the isolated-cylinder calculation. This is examined in figure 21.

The maximum heat-transfer coefficients on the cylinder are expressed as a fraction of the value calculated for the stagnation line of an infinite cylinder at zero sweep. Experimental values are shown by faired curves for $M = 9.6$ at three stations, and at $M = 8.1$ from the AEDC B-2 tunnel by the circles. At low angles of attack, up to about 20°, the Mach 9.6 data show a small effect due to the proximity of the nose at the station 1 diameter away from the shoulder, but beyond 3 diameters the heat transfer is independent of distance from the nose within the experimental scatter for both sets of data. Above 20°, however, the $M = 9.6$ data show the development of a distinct trend with distance from the nose.

Up to 20° the data also follow the trend with angle of attack predicted by the infinite-cylinder theory (ref. 6), but depart considerably from this trend at higher angles. In fact, the Mach 8.1 data indicate that the heat transfer actually decreases above about 40°. For angles of attack above 20°, the schlieren photographs of figure 3 show that the shocks are no longer parallel to the cylinder elements, as required for the application of infinite-cylinder theory. For this range, the flow pattern is dependent on the local span as well as on the cylinder diameter, and the "leading edge" must be treated as the round edge of a plate.

A brief overall view of the flow fields and heat transfer to the simple delta wing with laminar flow has been presented. An actual vehicle will, of course, be complicated by fins, controls, and other modifications, which will require detailed study, but the simple-delta-wing results can provide the basis for design of most of the vehicle surface. In spite of the lack of a general theoretical method for computing the flow field and heat transfer for the entire wing at angles of attack, a knowledge of the streamline patterns and pressures allows the prediction of the heat transfer by application of simple methods. Furthermore, these flow fields provide the basis for application of more elaborate theories for turbulent as well as laminar boundary layers.

CONCLUDING REMARKS

In summary, then, insofar as pressures are concerned successful correlations have been shown for both the center-line and spanwise pressure distributions over a range of sweep, Mach number, angle of attack, and dihedral angle. Such correlations allow the application of experimental results to Mach numbers widely different from those at which the data were obtained, thus allowing the prediction of the pressure on the lifting surface of a vehicle such as the Dyna-Soar with confidence. Much of the heat transfer has been found to be amenable to simple approaches which take into account the flow pattern peculiar to the angle-of-attack range under consideration. The leading edge itself has been found to

[redacted]

become a trailing edge in the sense of airflow direction at high angles of attack. This is connected with the appearance of conical flow on the delta wing and tends to alleviate the heat transfer to the leading edge.

Langley Research Center,
National Aeronautics and Space Administration,
Langley Field, Va., April 11, 1960.

L1042

[redacted]

REFERENCES

1. Chernyi, G. G.: Effect of a Small Blunting of the Leading Edge of a Profile on Flow Around It at High Supersonic Speeds. Library Translation No. 704, British R.A.E., Nov. 1957. (Available from ASTIA as AD 154789.)

2. Vaglio-Laurin, Roberto: Laminar Heat Transfer on Blunt-Nosed Bodies in Three-Dimensional Hypersonic Flow. WADC Tech. Note 58-147, ASTIA Doc. No. AD 155 588, U.S. Air Force, May 1958.

3. Phillips, William H.: Research on Blunt-Faced Entry Configurations at Angles of Attack Between 60° and 90°. NASA TM X-315, 1960.

4. Lees, Lester: Laminar Heat Transfer Over Blunt-Nosed Bodies at Hypersonic Flight Speeds. Jet Propulsion, vol. 26, no. 4, Apr. 1956, pp. 259-269, 274.

5. Bertram, Mitchel H., and Feller, William V.: A Simple Method for Determining Heat Transfer, Skin Friction, and Boundary-Layer Thickness for Hypersonic Laminar Boundary-Layer Flows in a Pressure Gradient. NASA MEMO 5-24-59L, 1959.

6. Beckwith, Ivan E.: Similar Solutions for the Compressible Boundary Layer on a Yawed Cylinder With Transpiration Cooling. NASA TR R-42, 1959. (Supersedes NACA TN 4345.)

7. Lawson, Warren A., McDearmon, R. W., and Rainey, R. W.: Investigation of the Pressure Distributions on Reentry Nose Shapes at a Mach Number of 3.55. NASA TM X-244, 1960.

8. Julius, Jerome D.: Experimental Pressure Distributions Over Blunt Two- and Three-Dimensional Bodies Having Similar Cross Sections at a Mach Number of 4.95. NASA TN D-157, 1959.

9. Cooper, Morton, and Mayo, Edward E.: Measurements of Local Heat Transfer and Pressure on Six 2-Inch-Diameter Blunt Bodies at a Mach Number of 4.95 and at Reynolds Numbers Per Foot Up to 81×10^6. NASA MEMO 1-3-59L, 1959.

L
1
0
4
2

[redacted]

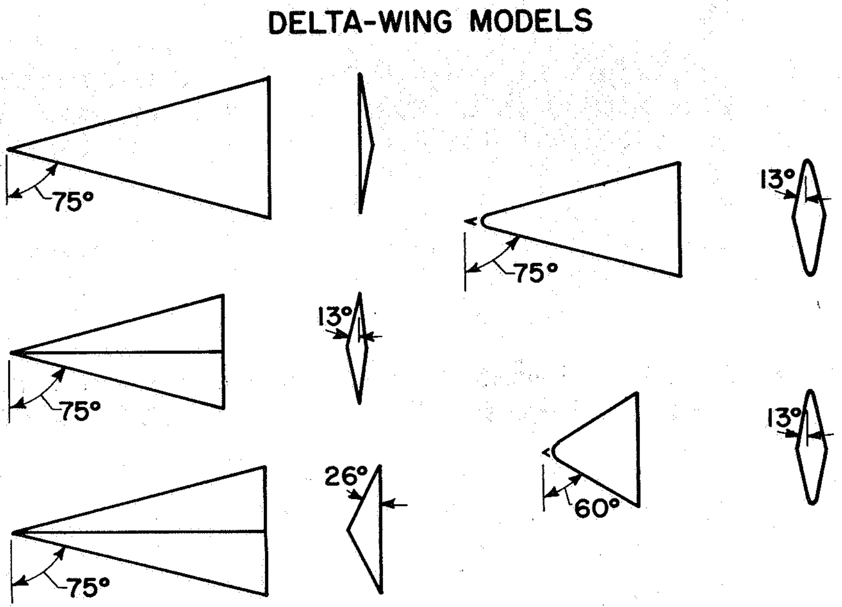
DELTA-WING MODELS
75°
75°
13°
75°
13°
75°
26°
60°
13°

Figure 1

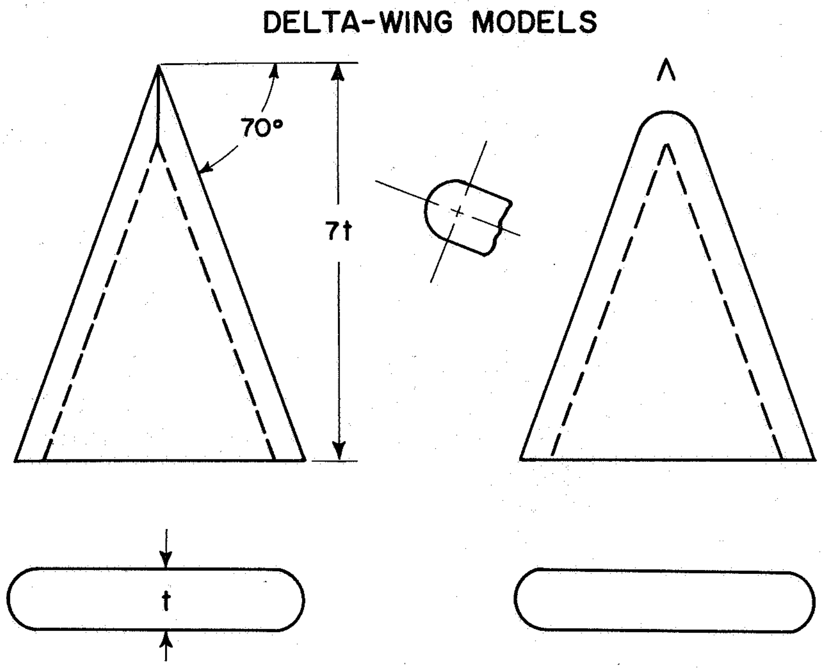
DELTA-WING MODELS
70°
7t
t

Figure 2

[redacted]

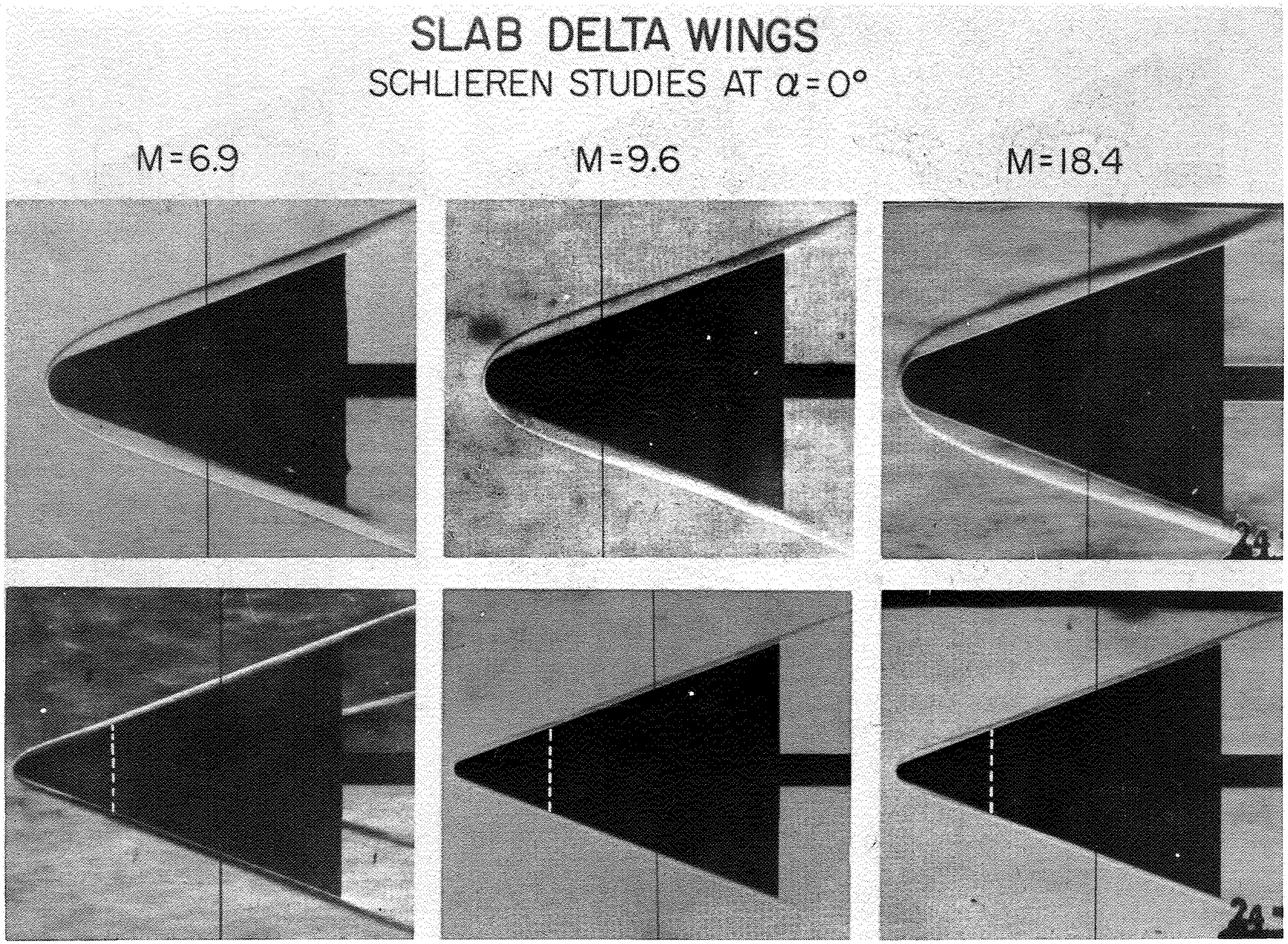
SLAB DELTA WINGS
SCHLIEREN STUDIES AT α = 0°
M = 6.9
M = 9.6
M = 18.4
24

Figure 3(a)

L-60-2467

[redacted]

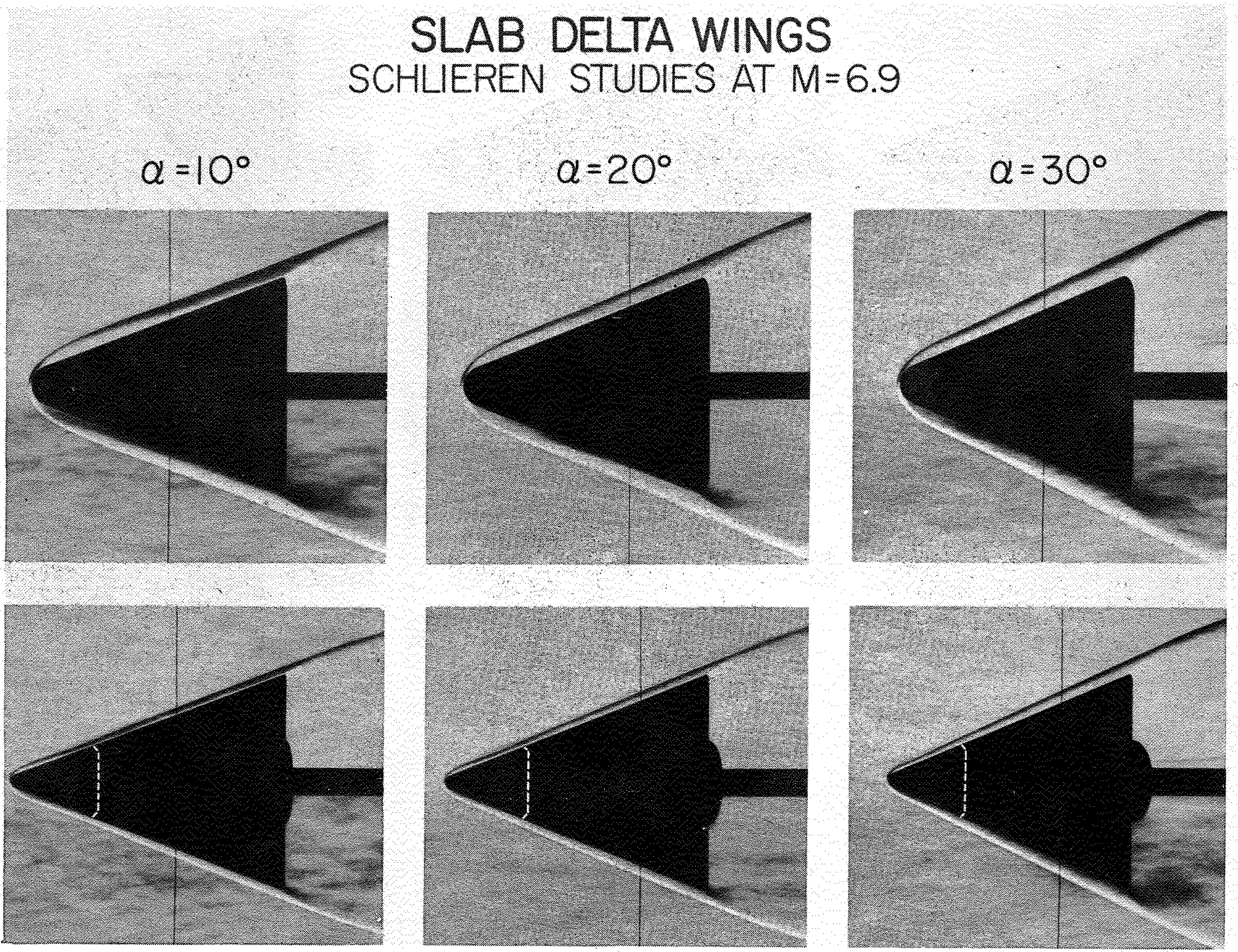
SLAB DELTA WINGS
SCHLIEREN STUDIES AT M=6.9
α =10°
α=20°
α=30°

L-60-2468

Figure 3(b)

[redacted]

[redacted]

EFFECT OF MACH NUMBER ON SHOCK ANGLE FOR FLAT DELTA WINGS

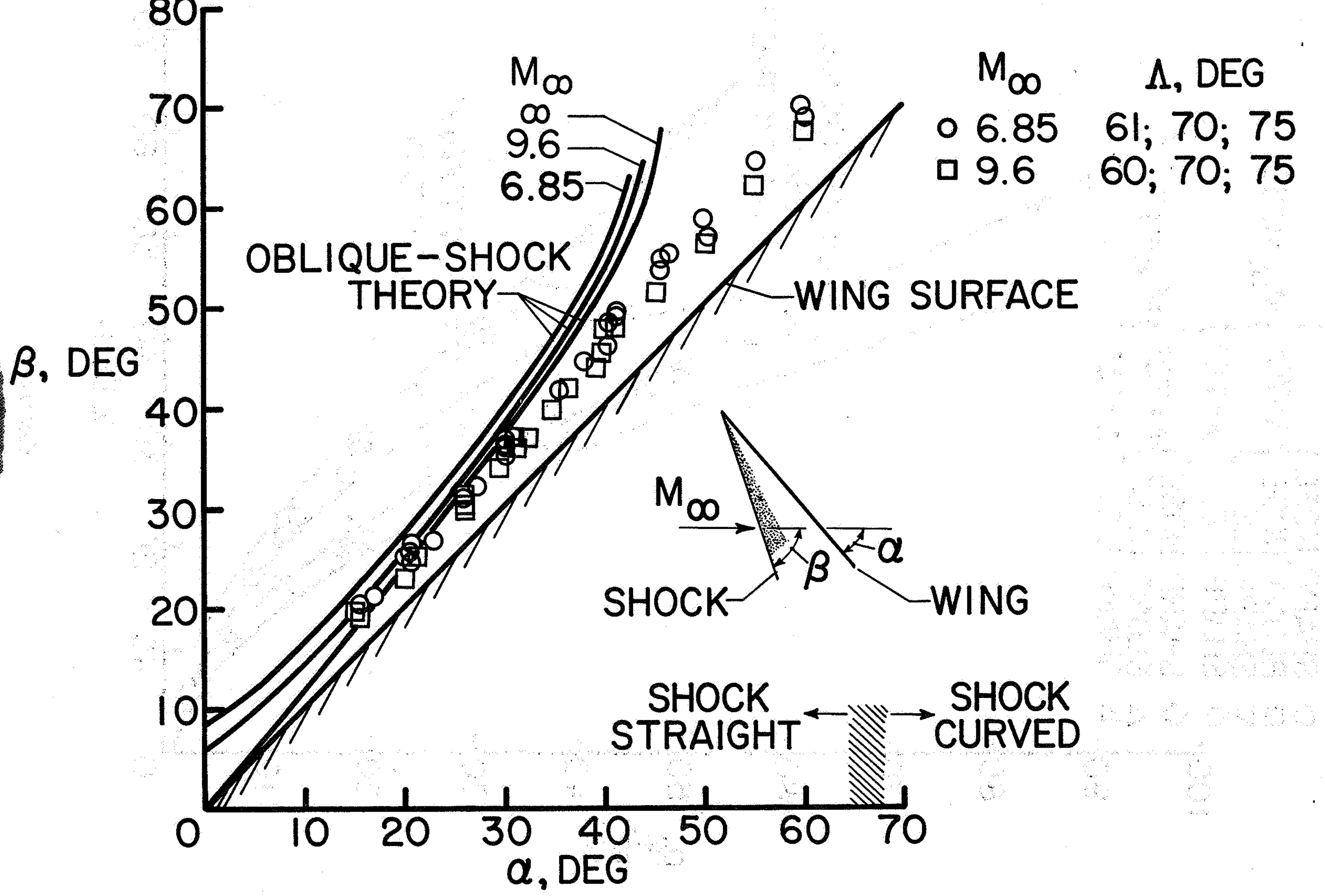

Figure 4

[redacted]

PRESSURES ON CENTERLINE OF FLAT DELTA WING

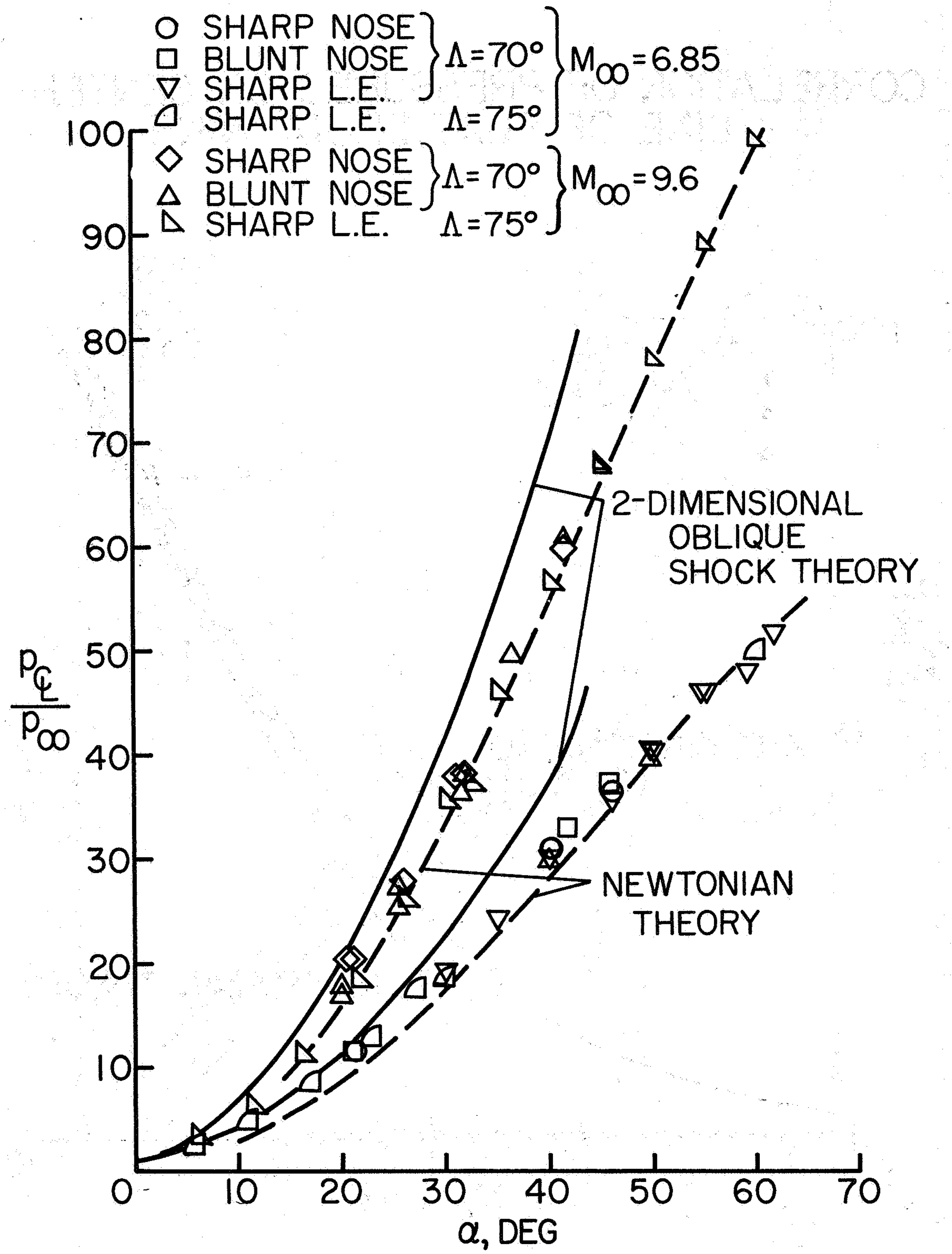

Figure 5

L-1042

[redacted]

L-1042

CORRELATION OF PRESSURES ON CENTER-LINE OF FLAT DELTA WING

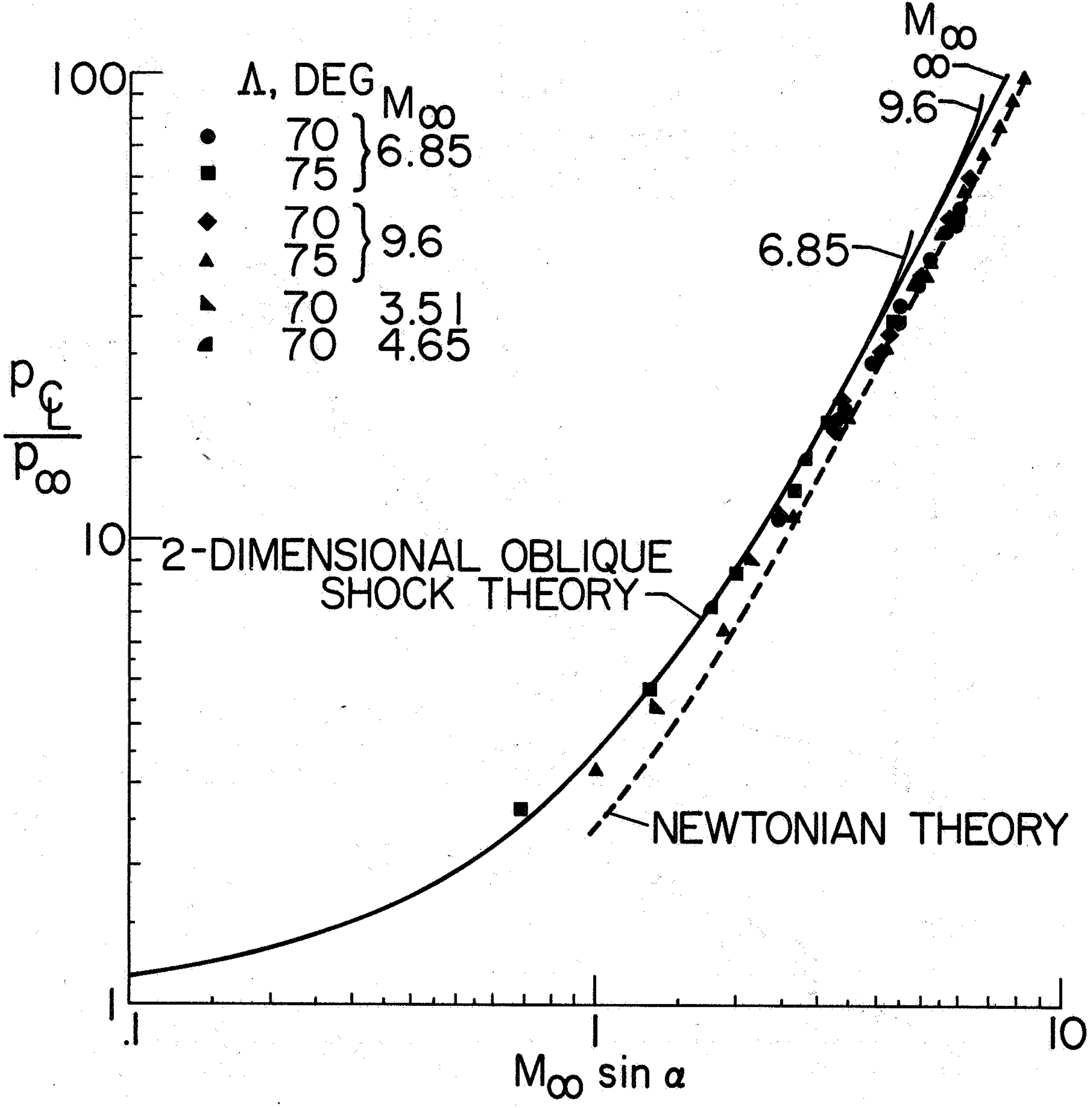

Figure 6

[redacted]

EFFECT OF DIHEDRAL ON SURFACE PRESSURES

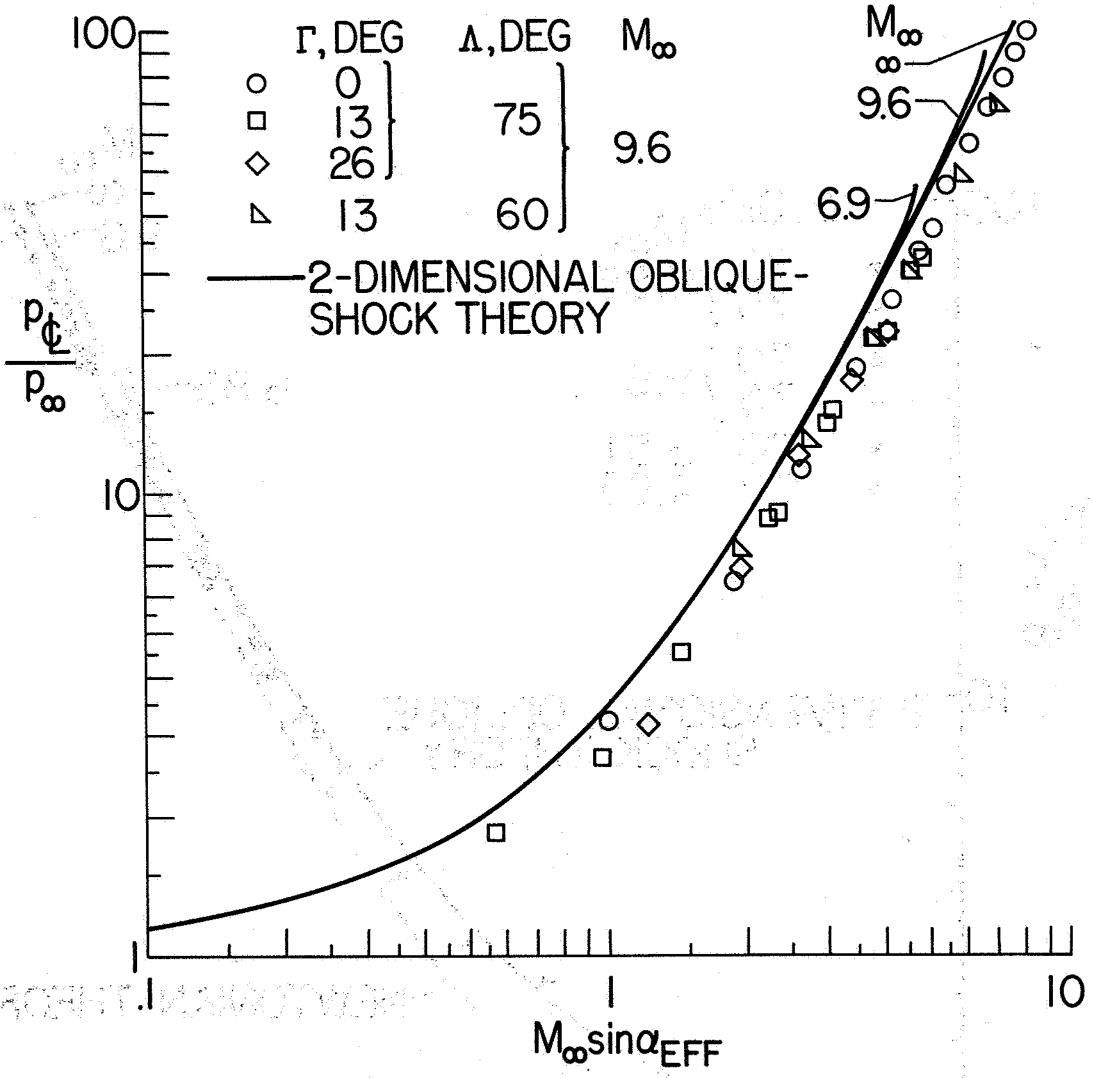

Figure 7

L-1042

[redacted]

CENTER-LINE DISTRIBUTION OF PRESSURE ON BLUNT DELTA WING

$\Lambda = 70°$

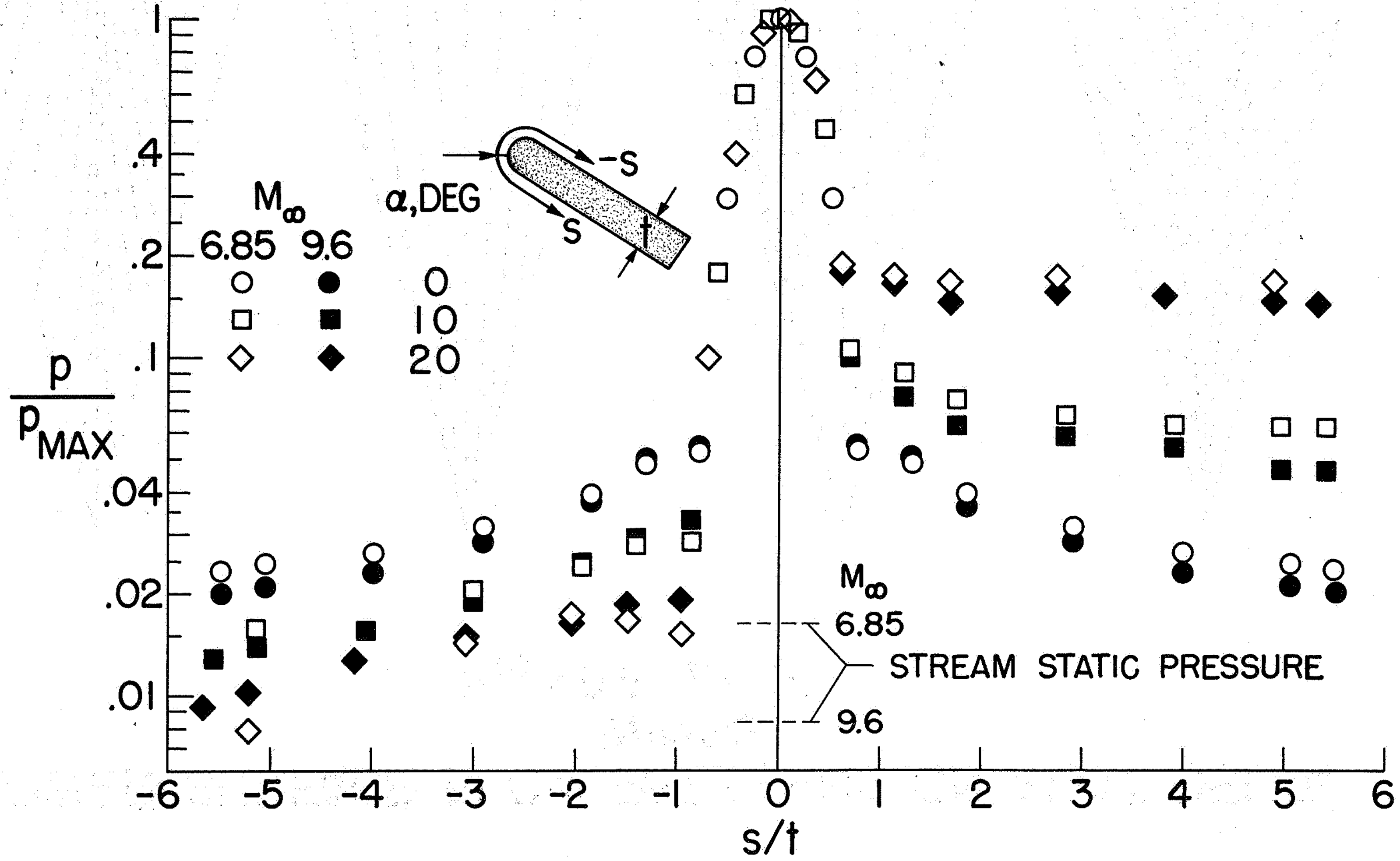

Figure 8

[redacted]

LOWER-SURFACE FLOW PATTERNS ON FLAT DELTA WINGS

$M_\infty = 9.6;\ \Lambda = 75°$

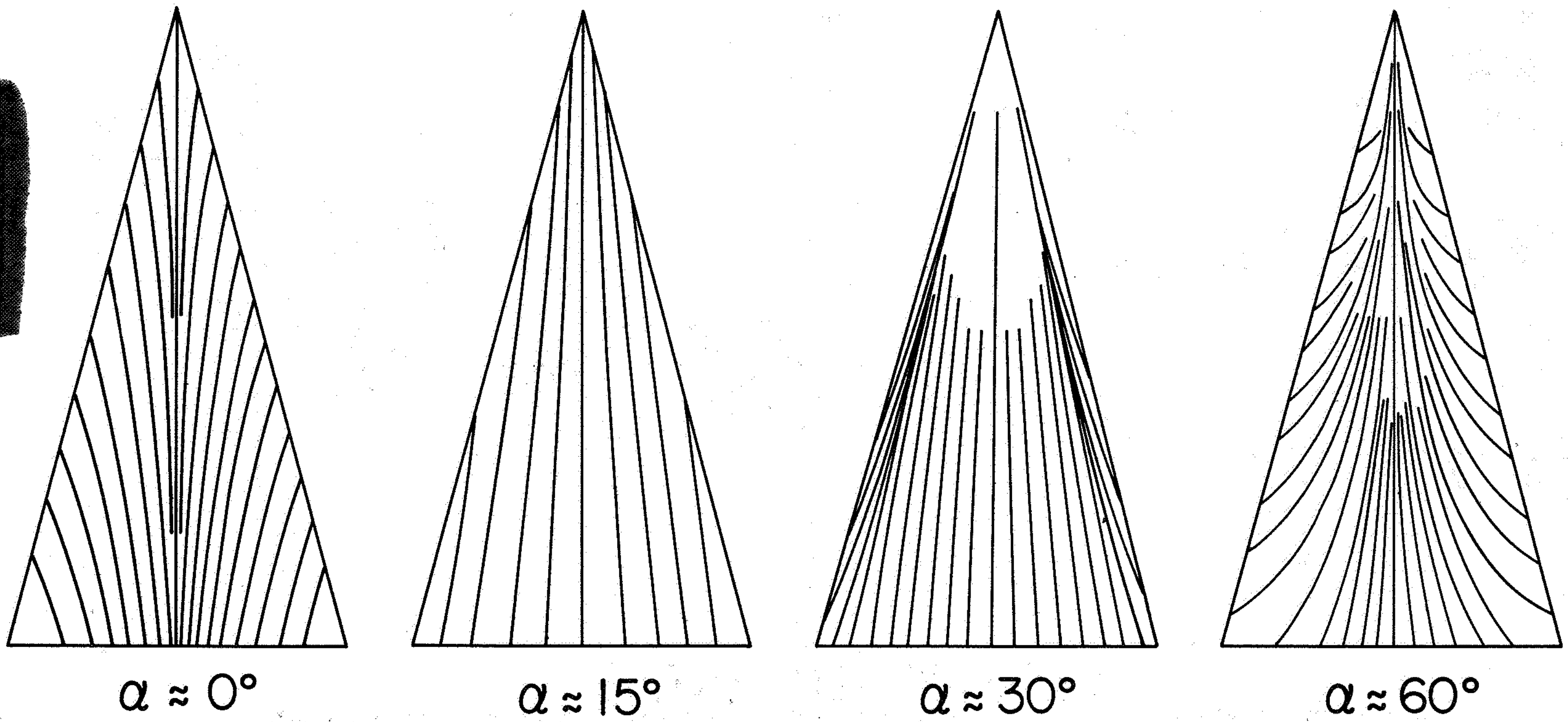
$\alpha \approx 0°$
$\alpha \approx 15°$
$\alpha \approx 30°$
$\alpha \approx 60°$

Figure 9

[redacted]

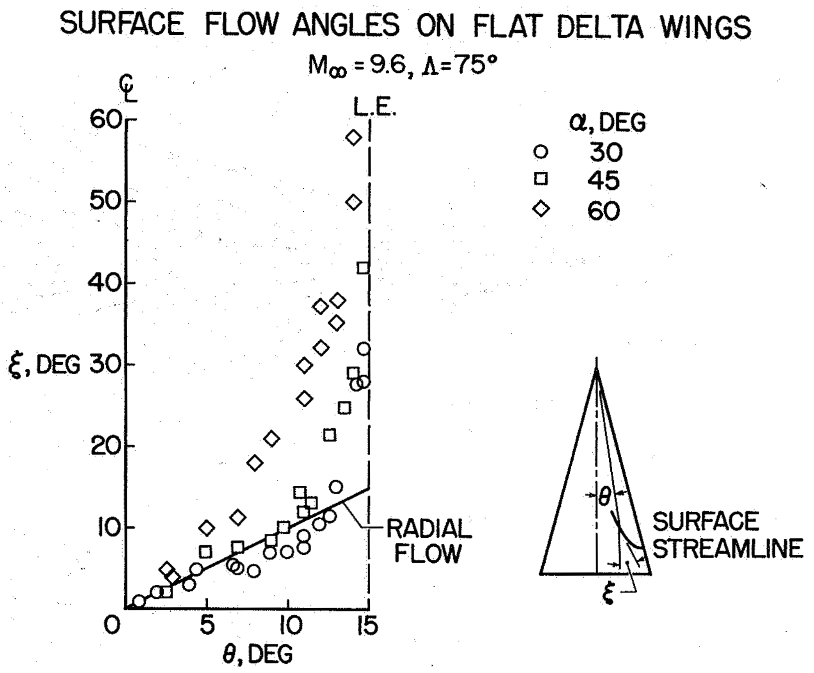

SURFACE FLOW ANGLES ON FLAT DELTA WINGS

$M_\infty = 9.6$, $\Lambda = 75°$

Figure 10

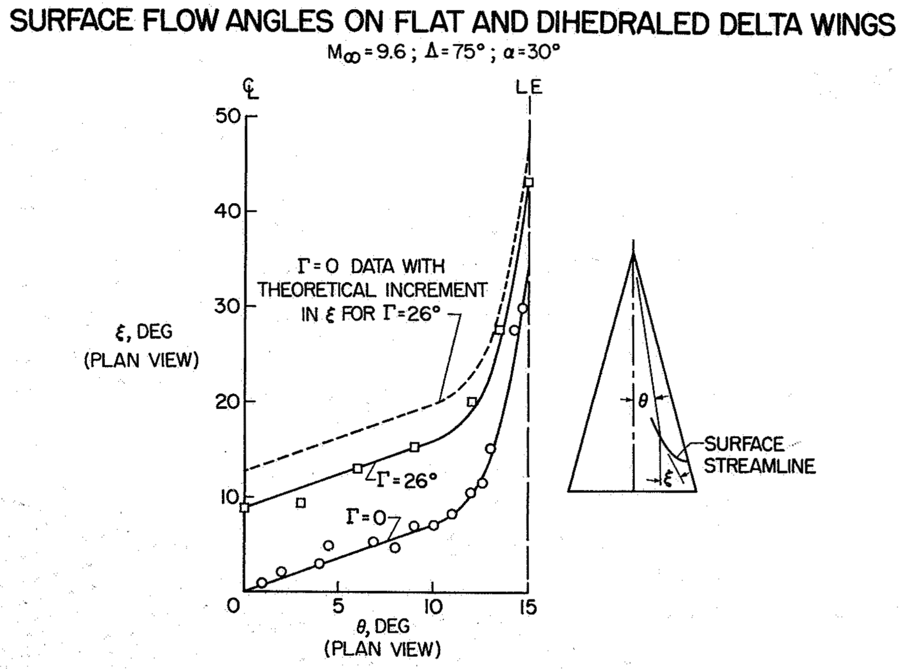

SURFACE FLOW ANGLES ON FLAT AND DIHEDRALED DELTA WINGS

$M_\infty = 9.6$; $\Lambda = 75°$; $\alpha = 30°$

Figure 11

[redacted]

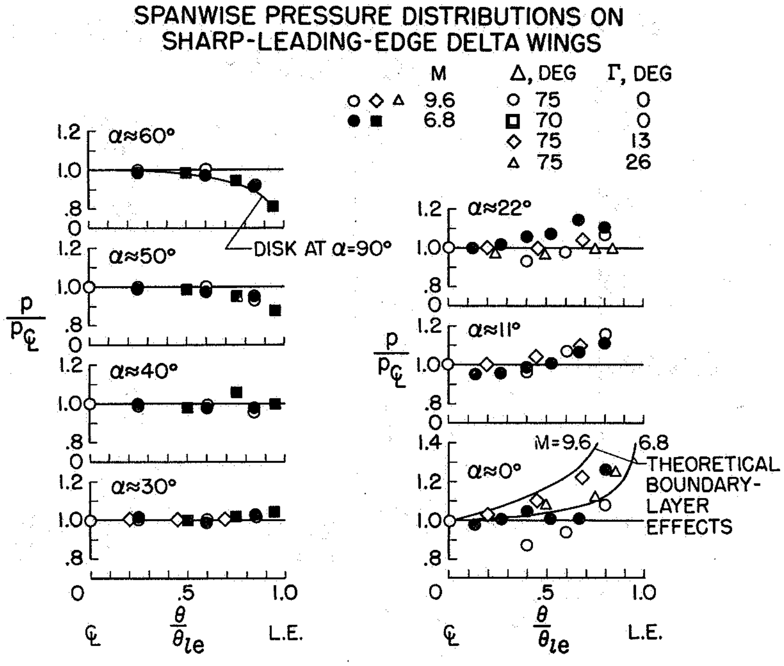

Figure 12

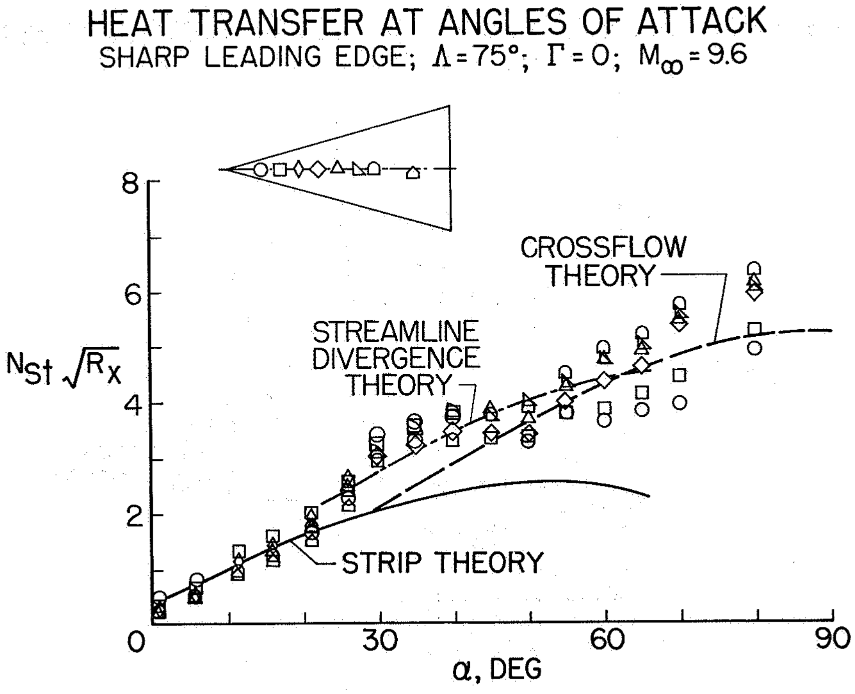

Figure 13

[redacted]

L-1042

[redacted]

EFFECT OF MACH NUMBER ON HEAT-TRANSFER DISTRIBUTION

SHARP-LEADING-EDGE DELTA WING ; $\Lambda = 75°$; $\alpha = 0°$

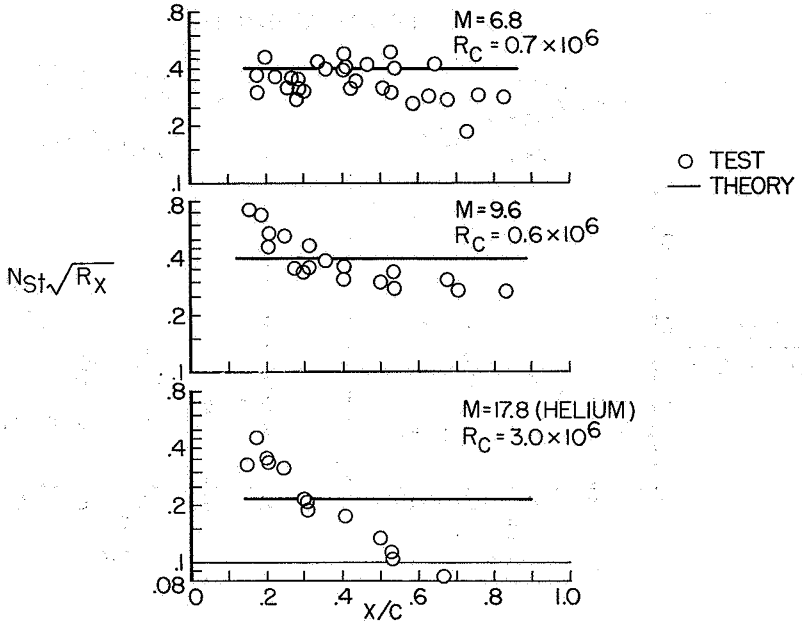

Figure 14

EFFECT OF MACH NUMBER ON FLOW PATTERNS AT $\alpha = 0$

SHARP-LEADING-EDGE DELTA WING ; $\Lambda = 75°$

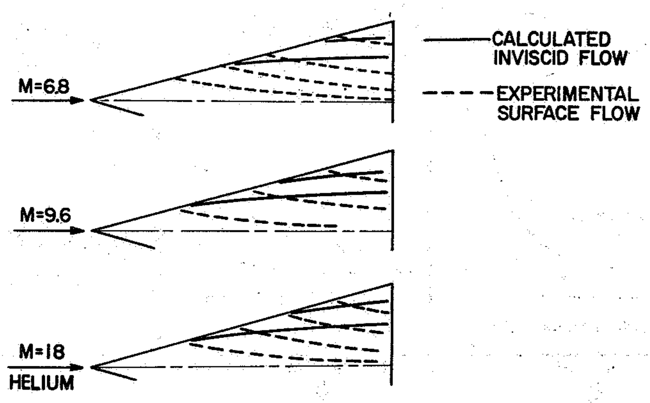
M=6.8
M=9.6
M=18
HELIUM
CALCULATED INVISCID FLOW
EXPERIMENTAL SURFACE FLOW

Figure 15

[redacted]

SPANWISE DISTRIBUTION OF HEAT TRANSFER AT ANGLES OF ATTACK

SHARP-LEADING-EDGE DELTA WING; $\Lambda=75°$; $M=9.6$; $R_c=0.6\times10^6$

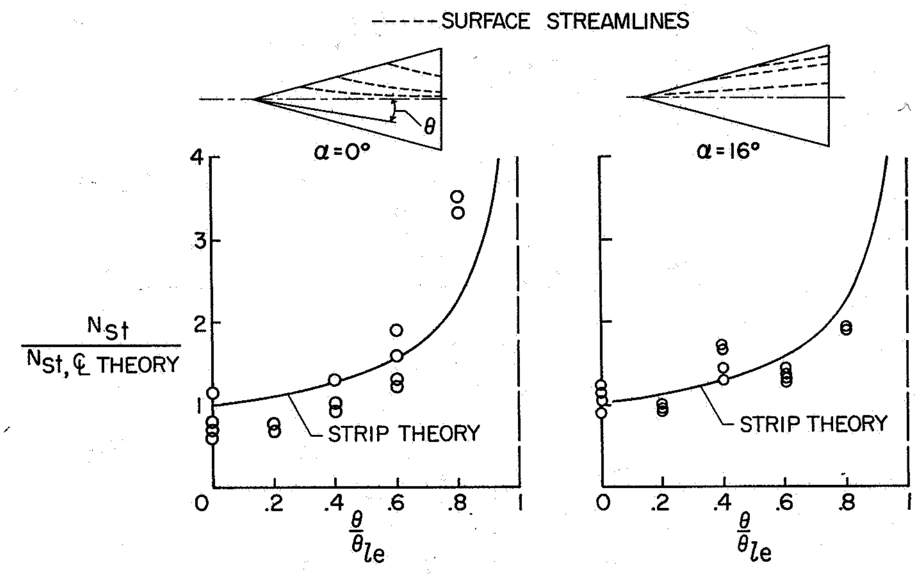

Figure 16

SPANWISE DISTRIBUTION OF HEAT TRANSFER AT ANGLES OF ATTACK

SHARP-LEADING-EDGE DELTA WING; $\Lambda=75°$; $M=9.6$; $R_c=0.6\times10^6$

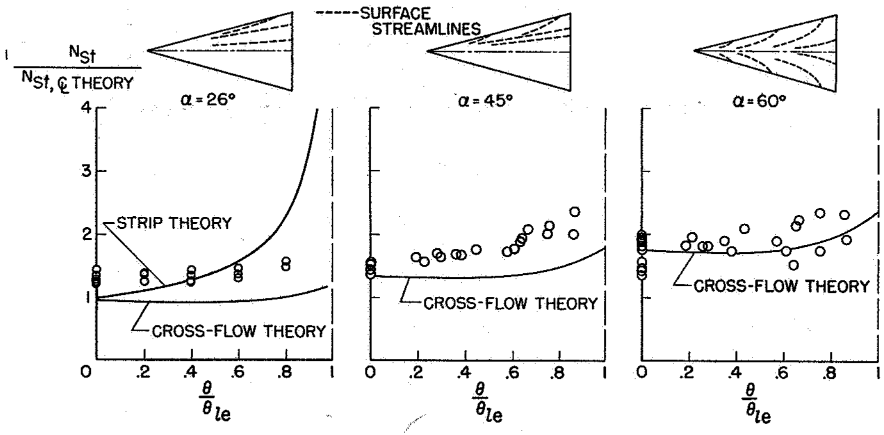

Figure 17

[redacted]

EFFECT OF DIHEDRAL ON HEAT TRANSFER TO DELTA WING

SHARP LEADING EDGE; $\Lambda=75°$; $M=9.6$; $R_C=0.6\times10^6$; $\alpha_{EFF}=26°$

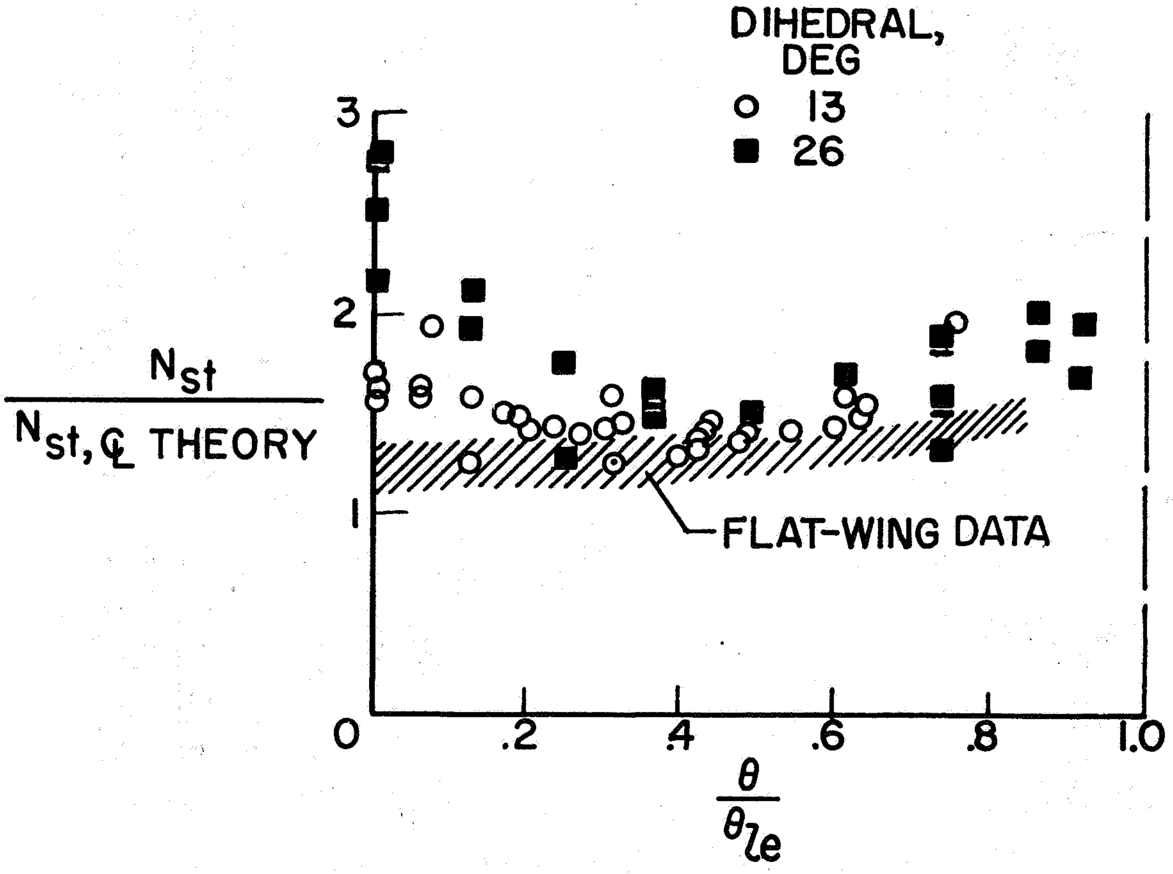

Figure 18

[redacted]

CENTER-LINE DISTRIBUTION OF HEAT TRANSFER ON BLUNT DELTA WING

Λ = 70°; CYLINDRICAL LEADING EDGE; SPHERICAL NOSE; M_∞=9.6

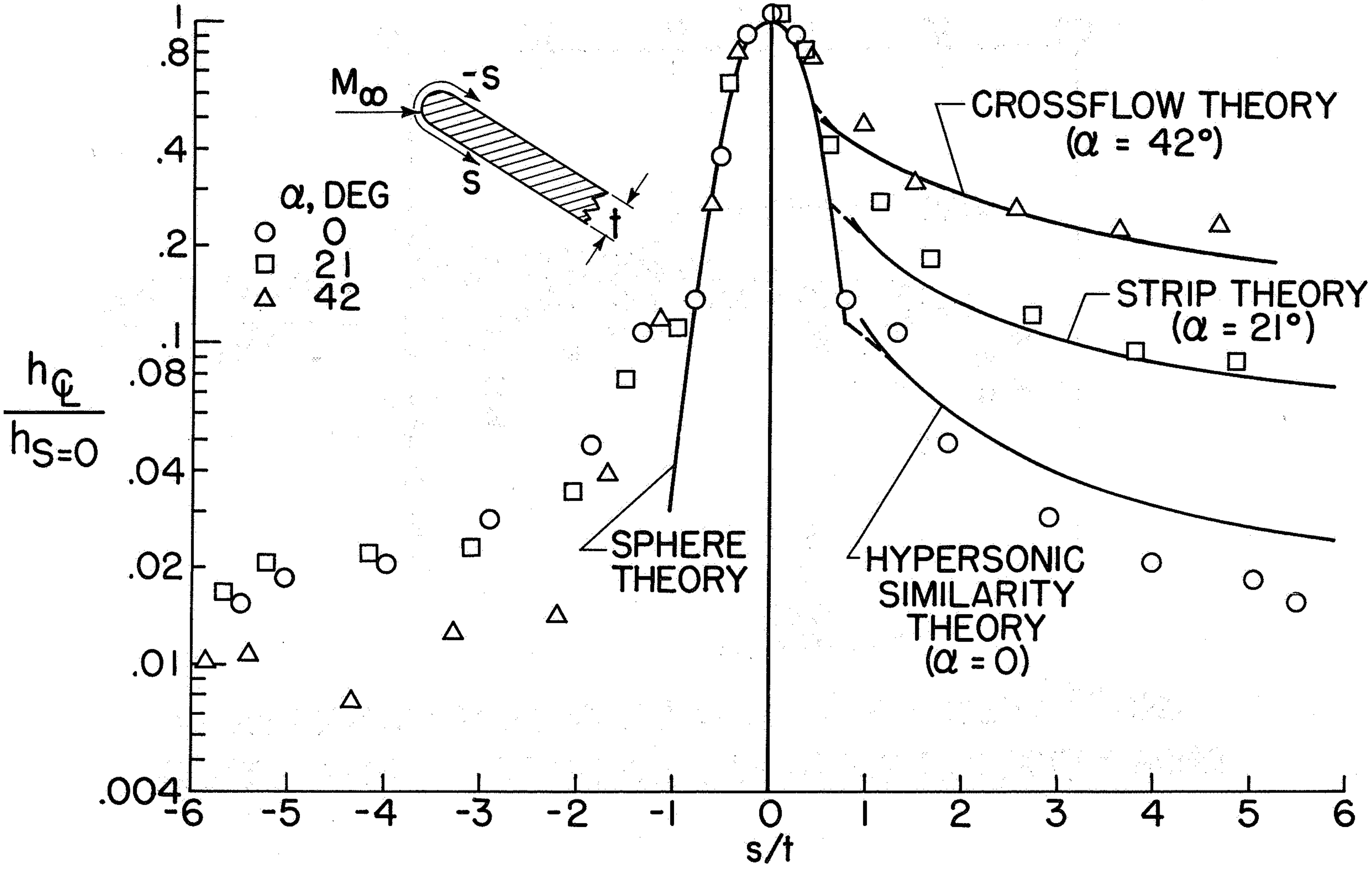

Figure 19

[redacted]

CORRELATION OF VELOCITY DISTRIBUTIONS ON FLAT-NOSED CYLINDERS

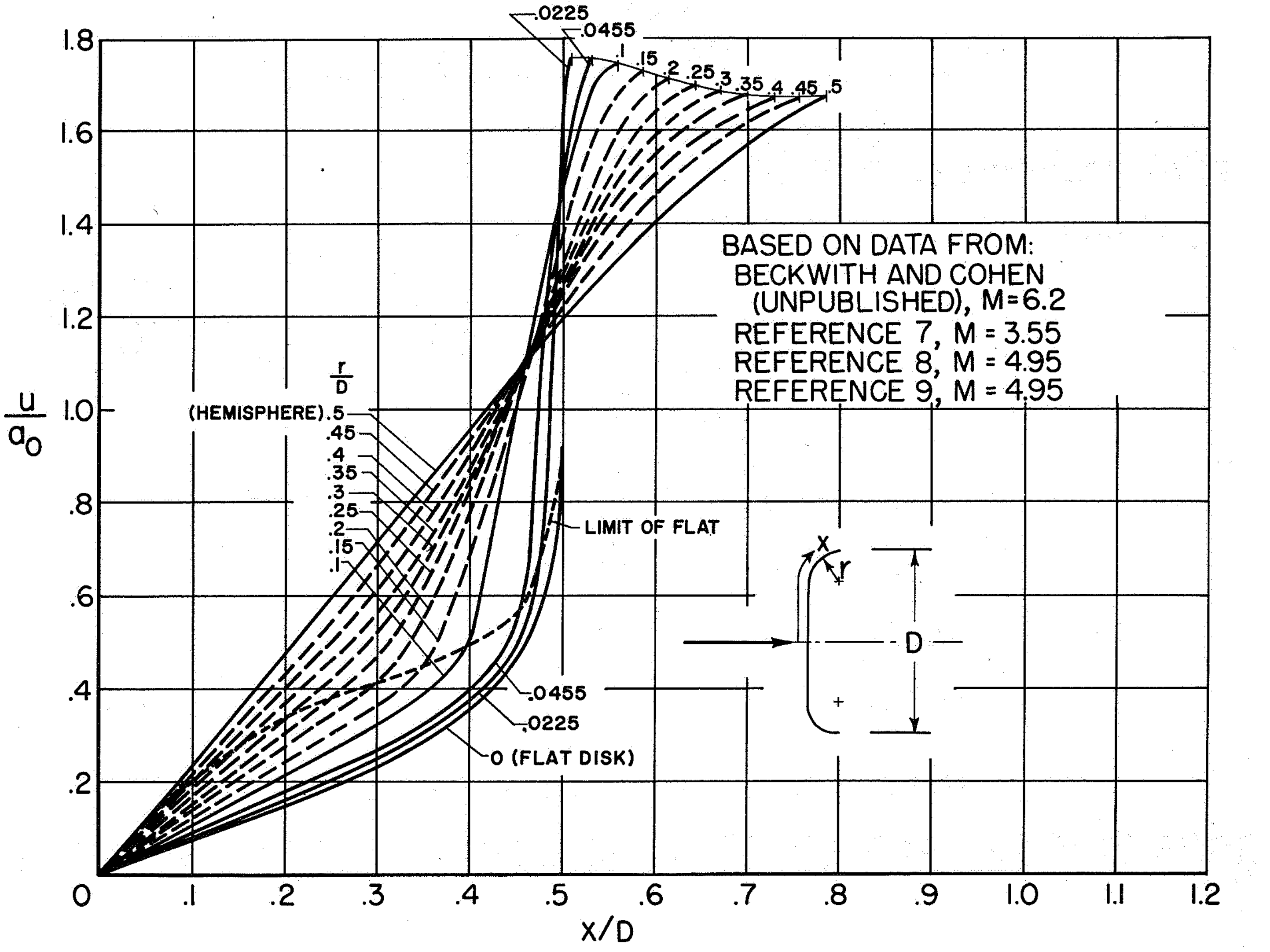

BASED ON DATA FROM:
BECKWITH AND COHEN
(UNPUBLISHED), M=6.2
REFERENCE 7, M = 3.55
REFERENCE 8, M = 4.95
REFERENCE 9, M = 4.95

Figure 20

[redacted]

MAXIMUM HEAT TRANSFER ON CYLINDRICAL LEADING EDGE

SPHERICAL NOSE; DELTA WING; $\Lambda = 70°$

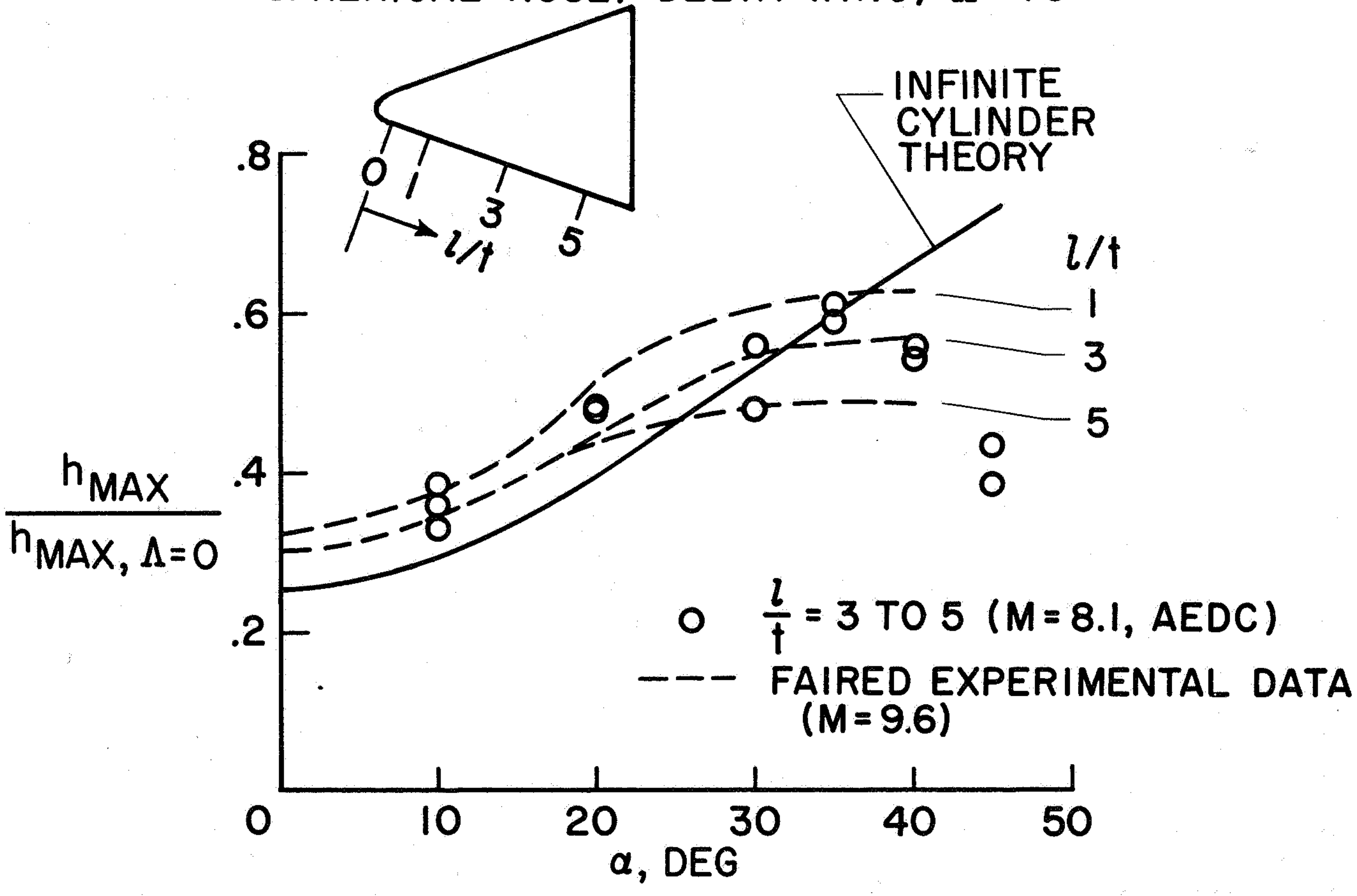

Figure 21

[redacted]

NASA - Langley Field, Va. L-1042

ERRATA

NASA Technical Memorandum X-316

By Mitchel H. Bertram, William V. Feller,
and James C. Dunavant
September 1960

Page 4, last line: Equation (1) is in error and should be replaced by the following equation:

$$\sin \alpha_{EFF} = \frac{\tan \Gamma \tan \theta_{1e} \cos \alpha + \sin \alpha}{\sqrt{1 + \left(\frac{\tan \Gamma}{\cos \theta_{1e}}\right)^2}} \tag{1}$$

NASA-Langley, 1962

Issued 1-4-62